Barunastra ITS for RoboBoat 2026: Nala Ares and Theseus Mark II

D. A. Briet, M. M. Miserideityo, J. N. Dikairono, D. V. Aubin, T. R. Nareswari, Y. K. Hendrata, R. M. Ansori, W. S. Nugroho, F. R. Akbar, W. N. Irawan, A. J. E. Caraka, K. N. Pratama, G. Y. Prawira, S. S. Rasendria, D. M. Suryono, B. H. Yudanto, M. R. Kurniawan, R. A. Maulana, I. S. Nugraha, A. Z. A. Prasetyo, R. I. Rasyad, N. P. Koroy, R. H. Putri, Z. N. A. Syamsudin, G. N. Anggalaksmana, P. N. A. Demetrias, S. R. Jatnika, V. A. Pandiangan, A. Talenta, R. Dikairono, L. Hakim, Muhtadin, M. I. Zazuli

Barunastra ITS RoboBoat Team, Institut Teknologi Sepuluh Nopember
Surabaya, Indonesia
barunastra.its@gmail.com

***Abstract*—This report presents the system design and technical strategy of Barunastra ITS for RoboBoat 2026. A Dual-Vessel Operation is implemented using two Autonomous Surface Vehicles (ASVs), Ares and Theseus, coordinated through a shared Robot Operating System 2 (ROS 2) framework to improve mission efficiency and coverage. Both vessels employ catamaran hulls with modular frame systems to support role-specific operation. Autonomous decision-making and navigation are structured through a layered control framework. System reliability is validated through staged testing, including virtual simulation, ground-level hardware checks, and on-water trials, ensuring readiness to consistently complete RoboBoat 2026 autonomy challenge missions.**

Acronyms and Abbreviations

ASV	Autonomous Surface Vehicle
GCS	Ground Control Station
MFE	Mel-Frequency Energy
MM	Mission Manager
PCB	Printed Circuit Board
ROS 2	Robot Operating System 2
SNR	Signal-to-Noise Ratio

I. Competition Strategy

A. General Strategy

This season, we aim to maximize efficiency through Dual-Vessel Operation, redeploying Ares and Theseus via a shared ROS 2 communication framework. While both prioritize mandatory missions, they fulfill distinct roles: Ares acts as the primary heavy-duty vessel capable of all tasks, performing LiDAR-based arena mapping and publishing the data. Complementing this, Theseus is optimized for speed and agility; lacking a LiDAR sensor, it subscribes to Ares' shared map and integrates it with GPS and computer vision to execute Tasks 3 and 6.

B. Mission Approach

Our mission strategy executes competition tasks sequentially while maintaining safety and robustness. A centralized Mission Manager (MM) controls task execution, state transitions, and priority handling for both vessels. Mission execution is tightly coupled to predefined navigation paths within the competition arena, enabling clear task boundaries and controlled interruption or resumption when required.

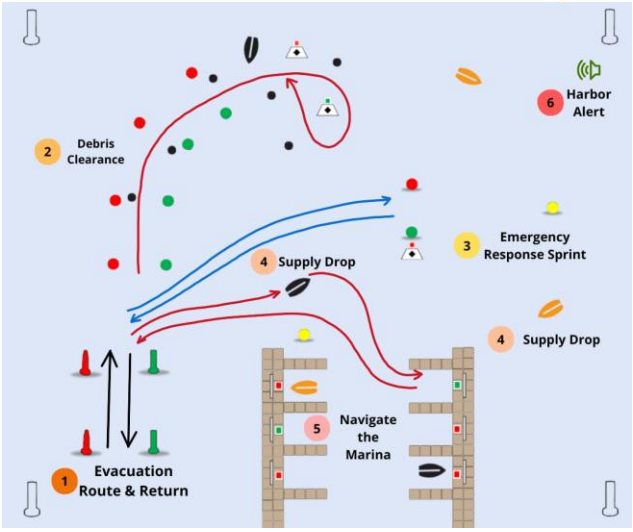

Fig. 1. Competition arena overview [1] with planned vessel trajectories: Ares (red), Theseus (blue), and shared paths (black).

As shown in Fig. 1, missions follow predefined navigation paths aligned with vessel roles: Ares operates along the red lines for endurance-focused tasks, Theseus follows the blue lines for agility-focused maneuvers, and the black lines denote missions common to all vessels using identical navigation logic. Mission execution may be interrupted by acoustic event detections, allowing the MM to suspend the current task, trigger a response mission, and resume nominal operation.

The initial objective requires passing through **Task 1 - Entry & Exit Gates**. Our logic defines a 'critical line' to isolate the navigation corridor and filters out objects outside this region. Navigation is then determined by the relative geometry of detected buoys: the vessel centers its heading at the midpoint of a gate or adjusts laterally if only a single buoy (port or starboard) is identified. The task is marked complete when no valid buoys are detected within the critical line.

Building on this navigation framework, the vessels advance to **Task 2 - Navigation Channel**, which requires heightened spatial awareness as the vessel navigates the red-green channel while treating black buoys as hard constraints for avoidance. A key feature of our approach is the 'search-and-circle' sequence; upon clearing the channel, the system applies universal obstacle avoidance to all detected objects while simultaneously searching for the green beacon. This allows for a controlled circling maneuver regardless of the red beacon's proximity. Finally, the return path utilizes inverted guidance logic for a precise channel departure.

This logic is further adapted for **Task 3 - Speed Challenge**. After passing the entry gate using Task 1 logic, the system identifies the color indicator to execute a half-circle maneuver. Once complete, the navigation parameters are inverted to guide the vessel accurately through the exit gate, finalizing the mission once the sensors confirm a clear path.

While transiting between these objectives, the system remains vigilant for **Task 4 - Object Delivery**. Upon identifying a target boat, the mission is added to the execution queue; the vessel will proceed to align with the required banner immediately after completing its current mission state. Once the distance threshold is reached and the delivery module is activated, the vessel retreats to continue its remaining navigation sequence.

For **Task 5 - Docking**, the vessel maintains a heading perpendicular to the dock, utilizing a lateral sway motion to scan the berths. During this traverse, dual cameras identify the lowest-numbered available berth while LiDAR ensures a safe standoff distance. Once selected, the vessel centers itself for entry, confirms success via proximity sensors, and executes a reverse maneuver to clear the area.

Operating in parallel with all missions, the system monitors for **Task 6 - Sound Signal**. Using a microphone, the system filters for specific frequency ranges before employing a machine learning classifier to identify signal types. These triggers initiate an immediate mission override, diverting the vessel based on the acoustic input. The MM tracks the interruption point, ensuring the vessel returns to its exact previous coordinates once the task is finalized.

Finally, for **Communications & Reporting**, the MM publishes mission data in JSON format over ROS 2. Each vessel receives this data, processes it, and reformats it according to predefined data structures. The reformatted mission data is then forwarded to the RoboCommand server using Protocol Buffers (protobuf) via the course network.

II. Design Strategy

A. Hull and Frame

The physical architecture of both vessels is based on a catamaran hull with an aluminum profile extrusion frame. Following the successful performance of Ares in the previous season, the Theseus platform adopts the same Aluminum Alloy 6063 extrusion framework, ensuring improved structural stiffness and load distribution. The extrusion-based design also enables modular hardware integration through a sliding-nut assembly, allowing rapid reconfiguration without permanent structural modifications.

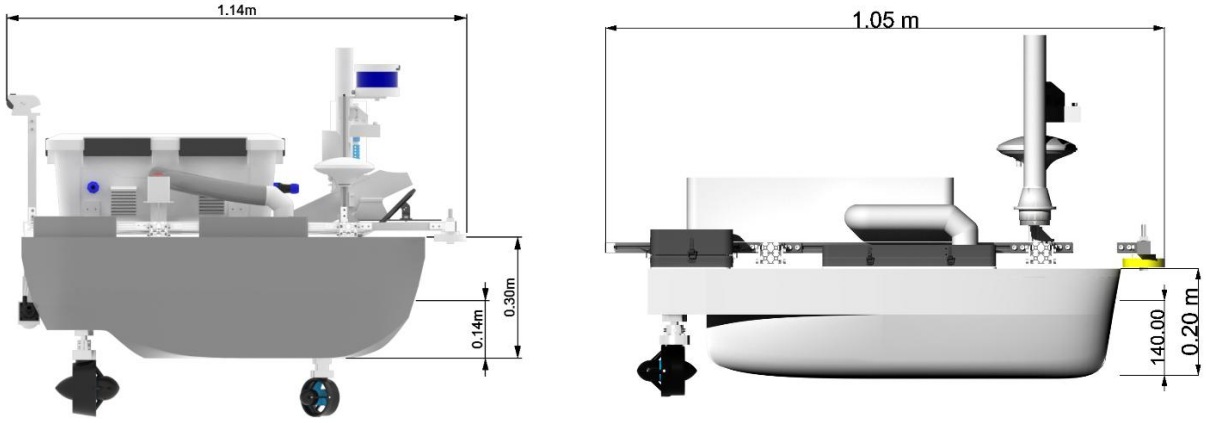

(a) (b)

Fig. 2. Side-view comparison of the (a) Ares and (b) Theseus catamaran hulls with principal dimensions.

A comparison of the hull dimensions of Ares and Theseus, shown in Fig. 2, reflects their distinct operational roles. Ares is configured with larger dimensions and displacement to accommodate its extensive sensor and mission-module to support a full mission completion. In contrast, Theseus adopts a smaller hull, reducing displacement and drag to attain high-speed and agile operation. The resulting dimensional differences arise from functional specialization, with detailed hull dimensions summarized in Table I.

TABLE I. PRINCIPAL DIMENSION COMPARISON

Specification	Vessels	
	Ares	***Theseus***
Length	0.99 m	0.88 m
Beam	0.86 m	0.68 m
Height Overall	0.90 m	0.90 m
Height	0.30 m	0.20 m
Draft	0.14 m	0.14 m
Block Coeff.	0.61 m	0.53 m
Demi-Hull	0.60 m	0.32 m
Displacement	31.77 kg	25.46 kg

B. Propulsion

The propulsion system is designed as a hybrid configuration to balance maneuvering with transit efficiency, allowing the vessels to adapt dynamically to mission requirements.

Ares utilizes a four-thruster setup. For station-keeping, it operates in a holonomic configuration (thrusters fixed at 45°) to provide simultaneous control of surge, sway, and yaw. During transit, it transitions to an azimuth-assisted mode by aligning the aft thrusters with the longitudinal axis to maximize forward thrust efficiency and reduce power consumption.

Unlike Ares, Theseus is designed for simplicity and electrical efficiency. It utilizes a differential thrust configuration with only two thrusters. This setup reduces the number of motor controllers and power demand, while providing reliable heading control and high-speed transit efficiency for missions that do not require omnidirectional movement.

C. Mission Modules

The vessel's hardware is outfitted with specialized modules to execute mission-specific tasks. These components facilitate the transition from sensor-based detection to physical actuation as detailed below:

1) Ball launcher: To overcome accuracy issues from previous seasons, the launcher was redesigned around two primary improvements.

a) Trajectory optimization: The launch angle was increased from 25° to 31°, ensuring a 0.55 m vertical clearance at a 1.5 m range. This specific configuration was selected over larger angles to minimize time-of-flight and environmental disturbances.

b) *Passive reloading:* We replaced the active servo system with a gravity-assisted mechanism. A 90° stock orientation contoured to the ball's geometry ensures consistent feeding, reduces mechanical complexity, and lowers power consumption.

2) Water shooter: To successfully complete the mission, we optimized the nozzle design to overcome jet range limitations observed in the previous season. By reducing the inlet diameter to 0.86 cm, this design maximizes fluid acceleration, achieving a pressure of 151 kPa and a velocity of 17 m/s to ensure a stable jet against wind resistance.

3) *Microphone:* To address the requirements of Task 6 - Sound Signal, we developed a detection system focused on robustness against unpredictable environmental noise through three fundamental elements.

a) *Acoustic extraction:* The system utilizes Mel-Frequency Energy (MFE) [2] for acoustic feature extraction. Compared to standard spectrograms [3], MFE provides superior energy representation within the 600, 800, and 1000 Hz domains while minimizing temporal-frequency resolution trade-offs. This prevents "blurring" of inter-blast gaps, ensuring accurate classification of the rapid sequences in two-blast patterns.

b) Neural network architecture: Rather than conventional filtering, we implemented Neural Network [4] architecture. This approach enhances adaptivity through data augmentation, allowing the model to reliably identify signals even as the Signal-to-Noise Ratio (SNR) degrades.

c) *Real-time processing*: Execution occurs on the onboard Mini PC, where the system is calibrated to detect step-like responses and impulsive transitions to ensure precise pattern recognition.

D. Electrical System

The electrical system provides reliable power distribution and communication between onboard components. Building on the custom-designed Printed Circuit Boards (PCBs) from last season, we refined trace routing and sizing to improve power stability and diagnostic visibility while maintaining compatibility with the existing architecture.

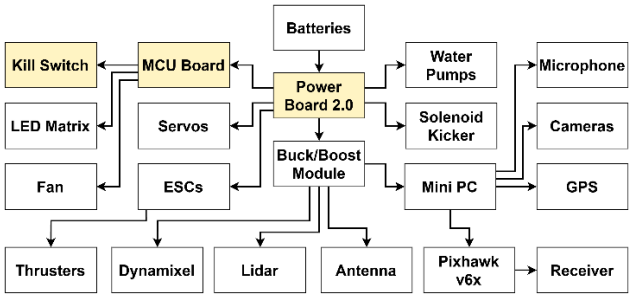

Fig. 3. Power architecture diagram with custom PBCs indicated in yellow.

As shown in Fig. 3, the system is centered around the Power Board 2.0, a custom PCB that integrates power regulation and distribution for all major subsystems. This centralized design simplifies wiring and enables consistent monitoring across sensors and actuators.

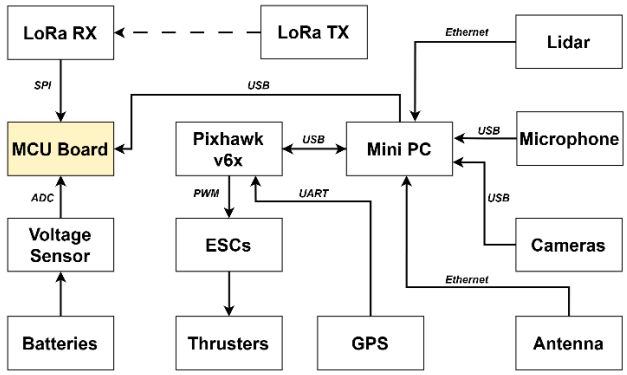

Fig. 4. Communication architecture diagram.

The communication architecture follows a hierarchical structure, with a Mini PC handling high-level autonomy and a Pixhawk responsible for low-level control. The MCU Board, which utilizes an STM32F411CEU6, manages safety-critical functions, specifically processing the battery voltage sensor data and executing the emergency kill switch logic. Isolating these tasks from the main computer ensures reliable safety operation independent of high-level compute load.

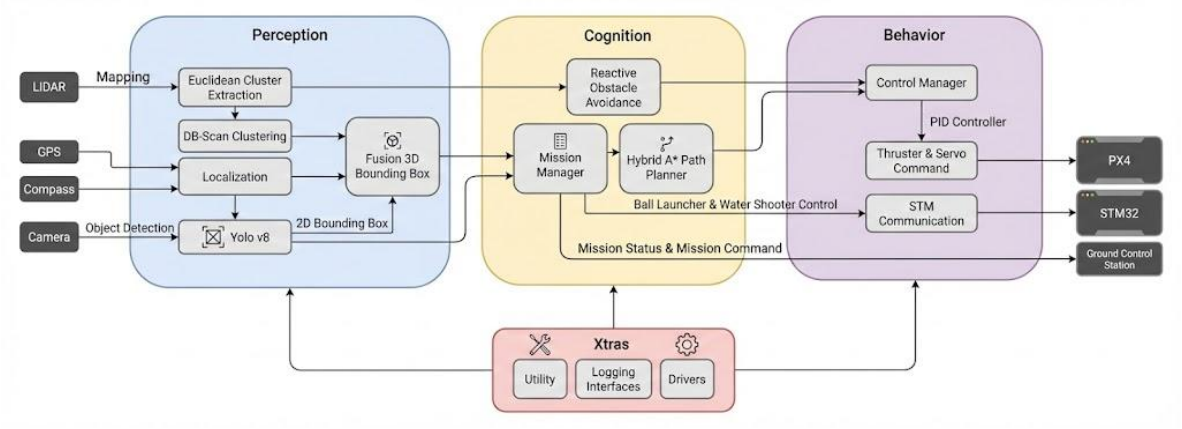

Fig. 5. Software architecture diagram.

E. Software Architecture

The system is built on ROS 2 Jazzy, serving as the framework for managing parallel execution and distributed communication between onboard modules and the Ground Control Station (GCS). The architecture is organized into four distinct modules:

1) Perception module: Acts as the sensing layer, responsible for acquiring and fusing data from onboard sensors. Camera-based object detection identifies mission-relevant objects, while LiDAR data is processed via Euclidean cluster extraction [5] to localize obstacles in 3D space. Global positioning is achieved by fusing GPS, IMU, and compass data, allowing the system to transform local object detections into global coordinates for accurate mission reporting. Additionally, acoustic signals are captured via an onboard microphone and processed on the Mini PC using a machine-learning–based classifier.

2) *Cognition module:* Acts as the central decision-making layer, managing mission-specific logic and path planning by consuming data from the Perception module to generate high-level commands for the Behavior module. It features an MM that handles mission sequencing, state transitions, and high-priority interrupts for acoustic tasks. For navigation, the module implements Braitenberg-vehicle logic [6] for reactive obstacle avoidance and a Hybrid A* planner to generate feasible paths. Additionally, it manages auxiliary commands for object delivery tasks and generates mission status reports transmitted to the GCS for forwarding to the RoboCommand network.

3) *Behavior module:* Responsible for translating high-level commands into low-level hardware control. A control manager processes target inputs from the Cognition module through speed and angle controllers to generate precise actuation signals. Depending on the active mission from the MM, the vessel can operate in azimuth, differential, or holonomic motion modes. Thruster and servo commands are transmitted to the PX4 flight controller via uXRCE-DDS over Ethernet, ensuring direct and efficient communication between ROS 2 and PX4 topics. Commands for object delivery are sent separately via serial communication to the STM32 microcontroller.

4) *Xtras module:* A support layer containing shared utility methods, logging tools, hardware drivers, and custom ROS 2 interface. This module reduces code duplication and ensures system-wide consistency across the Perception, Cognition, and Behavior layers.

To maximize operational efficiency, the primary vessel shares LiDAR-generated map data with the secondary vessel via ROS 2 topics. This allows the secondary vessel to navigate complex environments using shared spatial data, compensating for its lack of dedicated LiDAR hardware.

III. Testing Strategy

Due to a condensed timeline of only two months, with just six weeks of active operational days, our testing strategy was designed for maximum efficiency.

To mitigate risks caused by unpredictable weather and limited field access, we conduct virtual testing to accelerate development and reduce reliance on physical trials. We develop our navigation and control software to support both simulation and physical deployment, enabling

similar modules to run in Gazebo and onboard the vessel. The simulation environment is designed to replicate RoboBoat 2026 tasks, allowing us to identify integration issues early and maintain a high level of consistency between simulated and real-world operations.

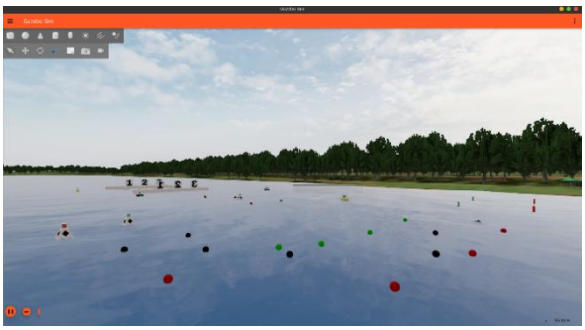

Fig. 6. Custom Gazebo simulation testing.

As part of perception evaluation, we benchmark multiple object detection architectures, including CNN-based YOLO and Transformer-based DETR [7]. All models are trained on the same dataset to assess the trade-off between detection accuracy and inference speed. This evaluation ensures that the selected model meets real-time performance requirements on the onboard hardware. The results of the comparison are presented in Appendix E.

Beyond visual sensing, we performed multi-stage testing of the acoustic system to ensure reliable detection of the specific frequencies. Initial evaluations using spectrogram-based features revealed limitations in resolving the short inter-blast intervals of the two-blast pattern, leading to misclassifications. Based on these findings, we adopted MFE feature extraction, providing improved temporal resolution and higher classification accuracy under low SNR conditions. Detailed performance results for both approaches are provided in Appendix D.

For physical validation, we apply a bottom-up testing approach that incrementally reduces technical risk from individual components to full system operation. This process includes structural and hardware verification, as well as communication testing to evaluate link reliability and latency between vessels and the GCS. This staged approach ensures that subsystem-level issues are identified and resolved before on-water deployment.

Fig. 7. On-water testing at InfinITS Park.

Final validation is conducted through on-water testing at the campus lake in InfinITS Park ITS, enabling evaluation under physical operating conditions beyond simulation. These trials expose the vessel to environmental disturbances such as lighting variations, wind, and wireless interference, allowing comprehensive assessment of the perception, control, and communication subsystems. On-water testing also supports evaluation of operational procedures, including system setup, calibration, and safety checks, ensuring system robustness prior to competition deployment.

ACKNOWLEDGMENTS

We would like to acknowledge the following institutions and partners for their support:

Dr. Rudy Dikairono, S.T., M.T., M.Sc., Muhtadin, S.T., M.T., and Lukman Hakim, S.T., M.T., for their guidance and advice to the team.

Nur Syahroni, Daniar Fahmi, Mila, Herlis, Maya Sari, Adifan, and Hafidz, from the Directorate of Student Affairs ITS, for their assistance with administrative requirements and official documentation related to competition funding release.

Junita Dwianingdijah of IKOMA (Ikatan Orang Tua Mahasiswa ITS), for her support in providing financial assistance for the competition.

PT Medco Energi Internasional Tbk. for the support via Cruise Package; PT Petrokimia Gresik and PT Pertamina Kilang Balikpapan for support via the Barge package; PT Dok Pantai Lamongan for support via the Sail package; and lastly Husky-CNOOC Madura Limited, Badak LNG, and Pelindo Marine Service for support via the Custom package.

REFERENCES

[1] RoboNation, “Section 3: Autonomy Challenge,” RoboBoat Resources, 2026.

[2] I. López-Espejo, R. C. M. C. Shekar, Z. -H. Tan, J. Jensen and J. H. L. Hansen, "Filterbank Learning for Noise-Robust Small-Footprint Keyword Spotting," ICASSP 2023 - 2023 IEEE International Conference on Acoustics, Speech and Signal Processing (ICASSP), Rhodes Island, Greece, 2023, pp. 1-5, doi: 10.1109/ICASSP49357.2023.10095436.

[3] A. P G and D. E D, "Epilepsy Detection using Spectogram data and Convolutional Neural Networks," 2023 14th International Conference on Computing Communication and Networking Technologies (ICCCNT), Delhi, India, 2023, pp. 1-6, doi: 10.1109/ICCCNT56998.2023.10307755.

[4] K. Mundada, A. Donge, A. Hursad, J. Ijmulwar and H. Ambekar, "Performance Analysis of Neural Network in Audio Recognition," 2024 International Conference on Recent Innovation in Smart and Sustainable Technology (ICRISST), Bengaluru, India, 2024, pp. 1-4, doi: 10.1109/ICRISST59181.2024.10921878.

[5] Point Cloud Library, “Euclidean Cluster Extraction,” PCL Documentation, n.d. [Online]. Available: https://pcl.readthedocs.io/projects/tutorials/en/master/cluster_extraction.html.

[6] S. Dvoretskii, Z. Gong, A. Gupta, J. Parent, and B. Alicea, “Braitenberg Vehicles as Developmental Neurosimulation,” arXiv preprint arXiv:2003.07689 [cs.AI], last revised May 11, 2022. [Online]. Available: https://arxiv.org/abs/2003.07689.

[7] N. Carion, F. Massa, G. Synnaeve, N. Usunier, A. Kirillov, and S. Zagoruyko, “End-to-End Object Detection with Transformers,” arXiv preprint arXiv:2005.12872 [cs.CV], last revised May 28, 2020. [Online]. Available: https://arxiv.org/abs/2005.12872.

Appendix A: Component List

Component	Vendor	Model/ Type	Specs	Custom/ Purchased	Cost	Year
ASV Hull	Barunastra ITS	Catamaran Hull	Carbon Fiber with LOA: 99 cm, Breadth (Hull only): 20 cm Height (Hull only): 30 cm Draft: 14 cm, Displacement: 31.77 Kg	Custom	$1532.00	2025
ASV Hull	Barunastra ITS	Catamaran Hull	Fiberglass with LOA: 88 cm, Breadth (Hull only): 18 cm Height (Hull only): 25 cm Draft: 14 cm, Displacement: 25.46 Kg	Custom	$1200.00	2022
Platform	Barunastra ITS	V Slot Extrusion	Aluminum Profile 20 x 20 1,52m, 20x40 2,38m V slot silver	Custom	$100.00	2026
3D Print	Creality	CR 10 MAX	Creality CR 10 MAX Datasheet	Purchased	Donated	2021
	BambuLab	A1	Bambu A1 Datasheet	Purchased	Donated	2025
	eSUN	PLA+	Amount:10 Rolls Diameter Size: 1.75mm Net Weight: 1Kg/spool	Purchased	$150.00	2026
Camera	Logitech	Webcam Brio 500	Brio 500 Datasheet	Purchased	$129.99	2025
	Dynamixel	MX-28	MX-28T/R/AT/AR	Purchased	Donated	2024
	U2D2	Power Hub Board	U2D2 Power Hub Manual	Purchased	$19.00	2023
	U2D2	Communication Converter	U2D2 Manual	Purchased	$32.10	2023
Communication	Ubiquiti	airMAX Omni Antenna AMO-5G10	airMAX Omni Antennas Datasheet	Purchased	$125.00	2025
	Ubiquiti	Power Beam 5AC Gen2 PBE-5AC	PowerBeam 5AC Gen 2 Datasheet	Purchased	$120.00	2025
	Ubiquiti	Rocket 5AC PRISM	Rocket Prism 5AC Gen 2 Datasheet	Purchased	$250.00	2023
Cooling System	DELTA	Brushless Fan 7x7 cm	DELTA Brushless Fan Datasheet	Purchased	$30.00	2024
CPU	ASUS	NUC Pro 14 Ultra 7	NUC PRO 14 Ultra Datasheet	Purchased	$575.36	2025
	ASUS	NUC Pro 12 i5	NUC Pro 12 Datasheet	Purchased	Donated	2025
GPS	Sparkfun	GNSS Multi-Band L1/L2	GNSS Multi-Band L1/L2 Datasheet	Purchased	$133.95	2024
	Sparkfun	ZED F9P	ZED-F9P-02B Datasheet	Purchased	$249.95	2024

LED Matrix	-	WS2812B 16x16 cm	Power Supply : DC 5V, SMD 5050, IC WS2812, Non Waterproof IP20,	Purchased	$12.50	2024
LiDAR	RoboSense	RS-16	RoboSense RS-16 Manual	Purchased	$700.00	2025
	Velodyne	Puck	Velodyne Puck Datasheet	Purchased	Vendored	2023
LoRa System	SEMTECH	Module LoRa SX1278	SX1276/77/78/79	Purchased	$5.50	2024
Microcontroller	STM32	STM32F4 11CEU6	STM32F411CE Datasheet	Purchased	$7.00	2025
	Arduino	Nano	Nano | Arduino Documentation	Purchased	$3.00	2025
Motor Controls	CUAV	Pixhawk V6X	CUAV Pixhawk V6X Controller	Purchased	$330.00	2025
Power System	OVONIC (Spare)	Lithium-Ion Polymer	4S2P 8200mAh 80C 14.8V	Purchased	$75.00	2022
	HOOVO (Spare)	Lithium-Ion Polymer	6S 6000mAh 60C 22.2V	Purchased	$80.00	2022
	ONBO (Main)	Lithium-Ion Polymer	4S 7200mAh 50C 14.8V	Purchased	$70.00	2023
	TATTU (Main)	Lithium-Ion Polymer	3S 2300mAh 45C 11.1V	Purchased	$23.00	2023
		Lithium-Ion Polymer	6S 10000mAh 25C 22.2V	Purchased	$159.00	2023
	Spectrum (Spare)	Lithium-Ion Polymer	3S 2200mAh 50C 11.1V	Purchased	$35.00	2024
	Zeee (Spare)	Lithium-Ion Polymer	6S 9000mAh 100C 22.2V	Purchased	$135.00	2024
Propulsion	Blue Robotics	T500	Blue Robotics Website	Purchased	$690.00	2024
	Blue Robotics	T200	Blue Robotics Website	Purchased	$200.00	2025
	APISQUEEN	U5	APISQUEEN Website	Purchased	$41.00	2026
	Blue Robotics	Basic ESC 500	Blue Robotics Website	Purchased	$110.00	2024
	APISQUEEN	45A bi-directional ESC	APISQUEEN Website	Purchased	$17.64	2026
	Savox	SB-2290SG	Savox Website	Purchased	$150.00	2024
Launcher System	uxcell	MQ8-ZI5B	Supply Voltage: 12V Bore Size: 1/2 #34 Diameter: 3 cm Primary Force: 10mm = 1000g Ultimate Force: 0mm = 1500g	Purchased	$10.00	2024
	Savox	SW-0231MG	Savox Website	Purchased	$50.00	2024
Teleoperation	Radiomaster	TX16S MKII Mark II	Radiomaster Website	Purchased	$200.00	2024

	Radiomaster	RP4TD ExpressLRS	Radiomaster Website	Purchased	$25.00	2024
Water Pump	Solar Water Pump	DC 12 V Water Pump 8 watt	Working Voltage: DC 12V Power Rating: 8W Max Water Height: 5m Max Flow: 10 L/min Diameter of Inlet: 15.5 mm Diameter of Outlet: 11 mm High quality solar water pump for DC current	Purchased	$5.00	2024
Waterproof Connectors	Zeatop Hendar	SP20 Aviation Connector	3P 20mm waterproof aviation Connector	Purchased	$6.00	2024
Algorithms	Barunastra ITS	-	-	Custom	-	2023
Localization and Mapping	Barunastra ITS	-	-	Custom	-	2025
Open-Source Software	ROS 2 Jazzy	-	-	Custom	-	2023
Vision	OpenCV	-		Custom	-	
Autonomy	Barunastra ITS	-	-	Custom	-	2025
Team Size	-	-	29	-	-	-
Testing time: simulation	-	-	Nov 23rd, 2025 – Jan 18th 2026	-	-	-
Testing time: in-water	-	-	Dec 16^{th}, 2025 – Feb 1st 2026	-	-	-
Hardware/Software expertise ratio	-	-	5:4	-	-	-

Appendix B: Test Plan & Result

TABLE I. TEST PLAN AND RESULT

Date	Objectives	Results	Location
11/23/2025 - 12/13/2025	- Virtual system validation using Gazebo simulator - Sound blast dataset collection and training for the Sound Signal mission (ground-based)	- System validated via Gazebo simulation and ground-based testing - Localization, LiDAR, IMU, and YOLO perception modules operated reliably under static conditions - Sound signal processing successfully detected target acoustic frequency; misclassification occurred at 600 Hz due to layout discrepancies - Full-scale competition arena installed and verified. Layout adjusted for lake geometry	Barunastra ITS Laboratory
	- Full course physical arena installation and layout verification		InfinITS Park, ITS
12/14/2025 - 12/20/2025	- Hull leakage inspection and ground validation	- No hull leakage observed. Electrical and software systems are stable. - On-water deployment demonstrated stable buoyancy, maneuverability, and reliable GCS communication. - Entry & Exit Gates and Navigation Channel missions executed successfully. Buoys detected and loitering behavior verified. - Light beacon datasets expanded and labeled for illuminated regions, improving detection consistency. - PID parameters tuned for accurate waypoint following and obstacle avoidance	Barunastra ITS Laboratory
	- Initial Ares on-water deployment - Mission-level testing: a. Entry & Exit Gates b. Navigation Channel c. Speed Challenge (Theseus on Ares) - Light beacon dataset collection and model training - PID tuning for the azimuth thruster configuration and obstacle avoidance		InfinITS Park, ITS
12/28/2025 - 1/3/2026	- Docking arena dataset collection and training - Weekly arena configuration adjustment - Docking mission validation - Integrated mission testing: a. Entry & Exit Gates b. Navigation Channel c. Speed Challenge (Theseus on Ares) d. Docking - PID tuning for the holonomic thruster configuration	- Docking dataset revealed challenges in long-range detection due to small beacons and similarity to vegetation. - Docking entrance and arena layout modified to improve feasibility. - Holonomic motion control enabled precise lateral and rotational docking using front/rear cameras. - Integrated mission testing confirmed navigation channel following, green/red beacon detection, banner detection, and optimal docking station selection. - Mission parameters and PID values refined to enhance docking reliability	InfinITS Park, ITS
1/4/2026 - 1/10/2026	- Object Delivery mission testing - Weekly arena configuration adjustment - Sound Signal mission on-water validation - Initial Theseus on-water deployment - Entry & Exit Gates and Speed Challenge testing on Theseus	- Object Delivery missions validated through accurate banner centering and mission parameter configuration. - Damaged arena components repaired before testing. - On-water Sound Signal validation robust against vessel-induced noise. Detection range limited by speaker power. - Manual and autonomous modes tested on ground and water. - PID parameters adjusted to support differential drive motion for Theseus missions	InfinITS Park, ITS
1/11/2026 - 1/17/2026	- Full-scale on-water mission testing for Ares and Theseus - Weekly arena configuration adjustment	- Full-scale missions executed under competition-like constraints: 5-minute preparation, 15-minute mission runtime. - Arena configurations randomized to expose ASVs to varying environmental and structural conditions. - Systems maintained stable communication, navigation, and mission execution, demonstrating overall robustness	InfinITS Park, ITS

Appendix B.1: Risk Management

TABLE I. RISK MANAGEMENT

No.	Risk Description	Root Cause	Potential Impact	Impact Level	Likelihood	Mitigation Strategy	Responsible Team
1	System overheats	Continuous high-power operation and limited cooling airflow	Degradation or failure of Mini PC and ESCs	High	Medium	a. Limit continuous high-throttle operation b. Improve ventilation and heat dissipation	Electrical
2	Hull water ingress during operation	Collision with floating obstacles or shaft tolerance issues	Increased drag, loss of buoyancy, potential system failure	High	Low	a. Conduct post-test hull inspection b. Apply waterproof sealing and reinforcement c. Perform controlled leak testing	Mechanical
3	Loss of communication with GCS	Radio interference, antenna misalignment, or connector degradation	Inability to monitor or intervene during mission execution	High	Medium	a. Use redundant communication channels b. Secure antenna placement c. Perform pre-deployment link testing	Electrical & Programming
4	Insufficient power endurance	Battery aging or unexpected current spikes	Premature mission termination	High	Medium	a. Select batteries with adequate safety margin b. Implement real-time voltage and current monitoring	Electrical
5	Perception failure due to lighting variation	Overcast weather, glare, or shadows affecting camera input	Object misclassification or mission failure	High	High	a. Augment dataset with varied lighting conditions b. Apply image preprocessing techniques	Programming
6	Navigation drift or unstable control	Sensor noise, electromagnetic interference, or poor parameter tuning	Inaccurate path tracking and mission deviation	High	High	a. Shield sensitive sensors b. Validate tuning through simulation and on-water trials	Electrical & Programming
7	Thruster performance degradation	Debris entanglement in impellers	Reduced maneuverability and mechanical damage	Medium	Medium	a. Install protective thruster guards b. Perform routine cleaning after testing	Mechanical
8	Mission mechanism malfunction (delivery / launcher)	Structural vibration or timing synchronization errors	Task execution failure	High	Low	a. Reinforce mechanical mounts b. Validate timing logic under dynamic conditions	Mechanical & Programming
9	Water-based actuator failure	Hose displacement or pump instability during maneuvering	Loss of task functionality	High	Low	a. Secure hose routing b. Prepare spare pumps and connectors	Mechanical & Electrical
10	Manual recovery failure	Depleted remote controller battery	ASV stranded during emergency conditions	High	Low	a. Conduct pre-test battery checks b. Prepare spare power sources	Electrical
11	Structural fatigue due to prolonged operation	Repeated vibration and cyclic loading	Frame loosening or component misalignment	Medium	Low	a. Perform periodic structural inspection b. Reinforce critical joints	Mechanical
12	Adverse weather during testing	Rain, wind, or reduced visibility	Invalid test results or hardware exposure	Medium	Medium	a. Schedule testing based on forecast b. Prepare waterproofing and contingency plans	General Manager

Appendix C: Hull and Frame Analysis

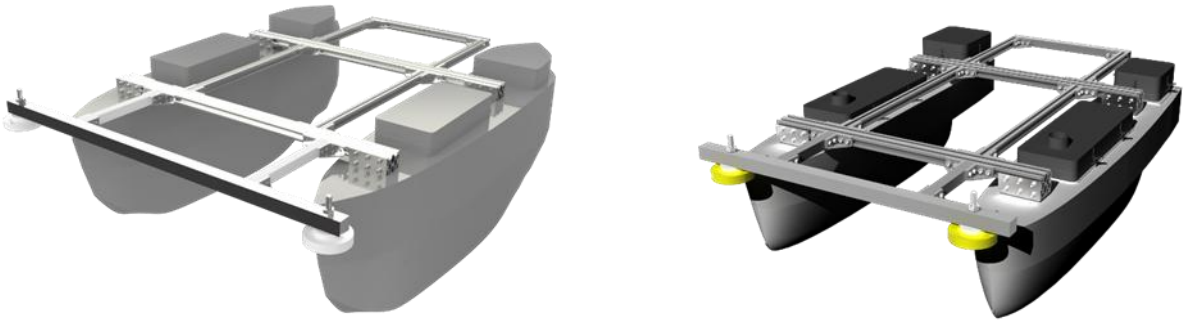

(a) (b)

Fig. 1. Hull and frame design of (a) Ares and (b) Theseus.

I. Introduction

This appendix details Ares and Theseus' hull and frame design and implementation, accommodating optimal autonomy performance for RoboBoat 2026.

II. Hull Design and Analysis

A. Ares' Hull Design and Analysis

There are a few changes made to the loadcase of Ares which makes the loadcase heavier than last year's competition. Some few changes are the added weight on the hull that helps Ares stabilize on rough waves area.

TABLE I. Ares' Loadcase Mass Calculation

Item	Qty.	Mass (kg)	
		Per Item	***Total***
Electrical Box	1	7	7
T500 Thruster	2	1.7	3.4
T200 Thruster	2	0.5	1
Battery S	2	1.3	2.7
Battery L	4	0.6	2.5
Frame	1	3.5	3.5
Water gun	1	0.2	0.2
Water pump	2	0.2	0.4
Lidar	1	0.8	0.8
Bumper	1	0.2	0.2
Omni Antenna	1	0.2	0.2
Radar	1	0.2	0.2
Camera	2	0.2	0.4
Ball Launcher	1	1	1
Camera frame	2	0.2	0.4
Lidar frame	1	0.1	0.1
Dry Ballast	2	1.5	3
Total Load			27

After the loadcase had been decided, its resistance was analyzed using ANSYS FLUENT to perceive the vessel drag force and wave making to determine all the component positions that can be seen in Fig. 2 and Fig. 3.

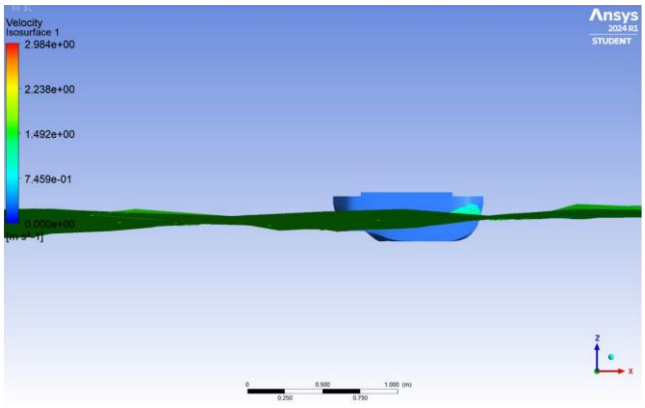

Fig. 2. Side view of Ares.

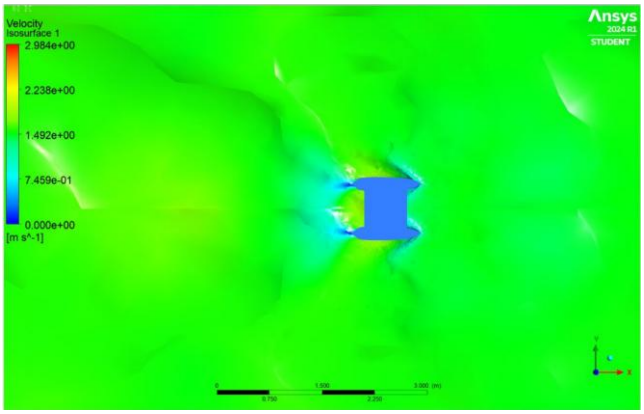

Fig. 3. Top view of Ares.

After we analyze the hull, we concluded that Ares' hull is still suitable for RoboBoat 2026 because the added mass doesn't really trouble the vessel ability to operate.

B. Theseus' Hull Design and Analysis

Theseus is projected to be the secondary vessel to collaborate with Ares in RoboBoat 2026. The vessel was designed to complete Task 1 and Task 3, hence the lighter loadcase shown in Table II.

TABLE II. THESEUS' LOADCASE MASS CALCULATION

Item	Qty.	Mass (kg)	
		Per Item	***Total***
Electrical Box	1	7	7
ApisQueen Thruster	2	1.3	2.6
Battery L	2	1.3	2.7
Battery S	1	0.7	0.7
Frame	1	2.5	2.5
Bumper	1	0.2	0.2
Omni Antenna	1	0.2	0.2
Radar	1	0.2	0.2
Camera	1	0.2	0.2
Camera frame	1	0.2	0.2
Total Load			16.5

After the loadcase was calculated, then the hull is analyzed using the loadcase as the added mass using Maxsurf Stability. The analysis was used to determine the safety of the vessel given the drastic loadcase difference from RoboBoat 2022 and RoboBoat 2026. After ensuring the stability of the vessel, we use ANSYS FLUENT to analyze the Hull Drag and Wave making of the vessel which can be seen in Figure 4.

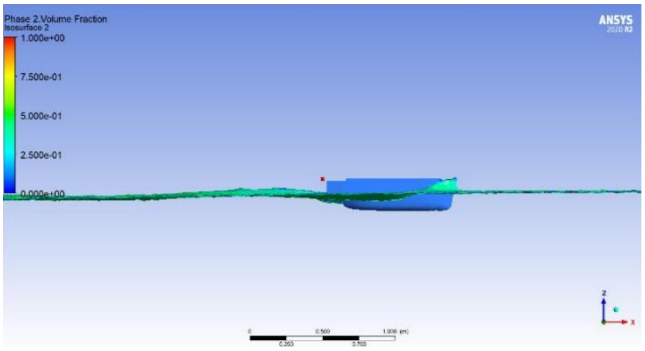

Fig. 4. Side view of Theseus.

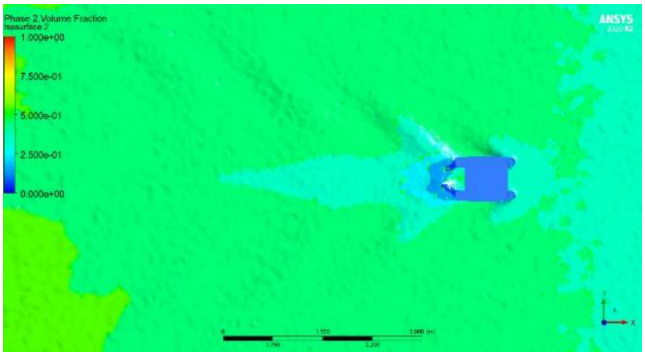

Fig. 5. Top view of Theseus.

III. FRAME DESIGN AND ANALYSIS

This section focuses on the design and analysis of the Theseus frame, as the Ares platform continues to utilize its proven framework with minimal structural changes. Theseus' frame has undergone significant redesign, transitioning from a lightweight Aluminum Hollow Bar to a V-Slot Aluminum Extrusion framework. This shift was driven by the need for greater structural stiffness and modular flexibility, effectively mimicking the successful architecture of Ares.

While the previous hollow bar construction was lighter, it was susceptible to bending under operational loads and offered limited mounting options. By adopting the extrusion-based design, Theseus now features a sliding-nut assembly, allowing for rapid component reconfiguration and easier maintenance without permanent structural modifications. Fig. 6 and Fig. 7 below showed the frame design comparisons between the older and newer version of Theseus.

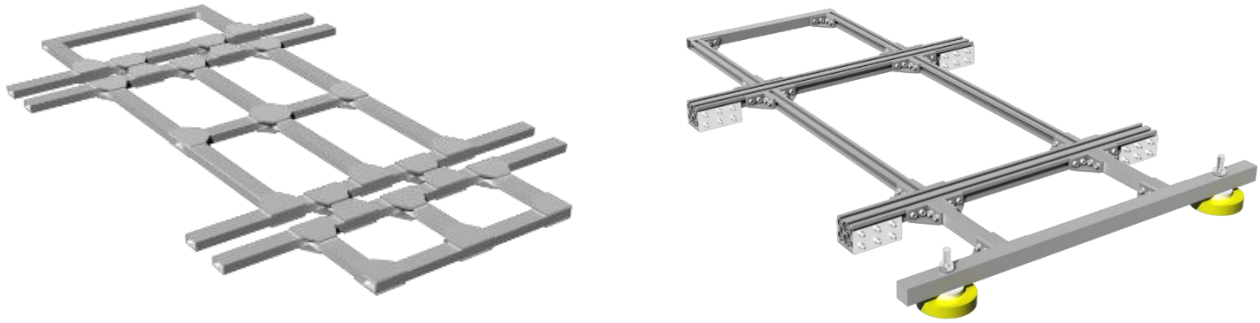

(a) (b)

Fig. 6. Theseus (a) old and (b) new main deck frame design.

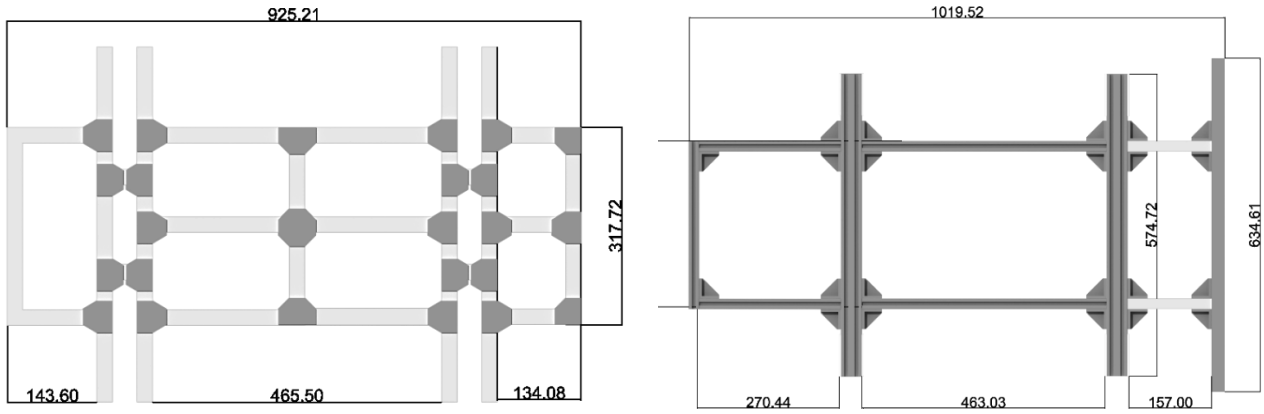

(a) (b)

Fig. 7. Theseus (a) old and (b) new main deck frame design with dimensions in millimeters.

The frame design then tested using ANSYS 2025 R1 Static Structural Mechanical Software. This software was chosen for the analysis since the loads which will be used are static and material behavior can be approximated as linear elastic. The static load will experience stress and deformation in steady-state condition, and this software is ideal due to its focus on static loading.

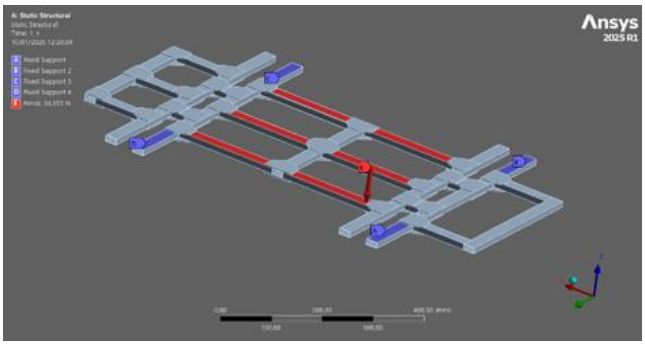

Fig. 8. Theseus old frame static structural analysis.

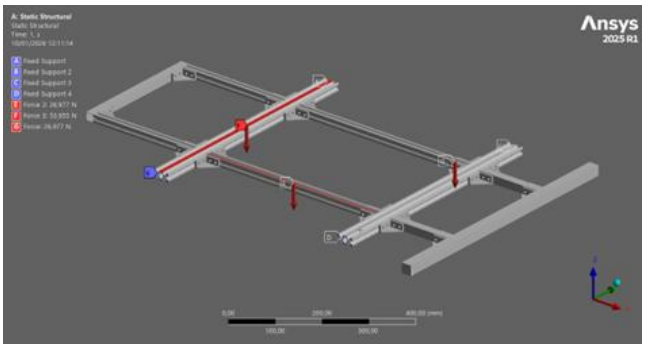

Fig. 9. Theseus new frame static structural analysis.

The analysis focused on key structural responses, including total deformation, equivalent (von Mises) stress, maximum principal stress, and minimum principal stress, in order to assess stiffness, stress distribution, and compressive stability. The results, summarized in the accompanying table, support the transition to the aluminum profile extrusion frame due to its

improved structural performance under the same simulation conditions.

TABLE III. FRAME STATIC STRUCTURAL COMPARISON

Parameter	**Frame Type**	
	Hollow Bar	***Extrusion***
Total Deformation (mm)	0,21122	0,033464
Equivalent (von-Mises) Stress (Mpa)	10,577	6,3178
Maximum Principal Test (Mpa)	11,551	1,9771
Minimum Principal Test (Mpa)	-10,705	-7,0834

Appendix D: Mission Modules

I. Introduction

This appendix provides a comprehensive technical breakdown of the methodologies, calculations, and experimental data used to address the RoboBoat 2026 mission requirements. While the primary report outlines our general strategy, the following sections detail the specific engineering solutions developed to ensure high-reliability performance across all tasks.

II. Ball Launcher

The objective of the current launcher is to hit a banner located at a horizontal distance up to x = 1.5 m with a target height of y target = 0.55 m. The muzzle height is assumed to be y0 = 0 (reference height aligned to the target's reference).

The trajectory is modeled using standard projectile motion equations in two dimensions:

$$x(t) = v_0 cos(\theta) \quad (1)$$

$$y(t) = y_0 + v_0 \sin\theta \; t - \frac{1}{2} g t^2 \quad (2)$$

To obtain an equation in terms of x rather than time t, time is eliminated using the horizontal motion:

$$t = \frac{x}{v_0 \cos(\theta)} \quad (3)$$

Substituting into the vertical equation yields the trajectory as a function of horizontal distance:

$$y(x) = y_0 + x \tan(\theta) - \frac{g x^2}{2 v_0^2 \cos^2(\theta)} \quad (4)$$

Defining the vertical offset to the target as:

$$\Delta y = y_{\text{target}} - y_0 \quad (5)$$

the target condition becomes:

$$\Delta y = x \tan\theta - \frac{g x^2}{2 v_0^2 \cos^2(\theta)} \quad (6)$$

Using the identity $\sec^2\theta = 1 + \tan^2\theta$ and solving the resulting quadratic in tan θ, the closed-form solution is:

$$\tan\theta = \frac{v_0^2 \pm \sqrt{v_0^4 - g(g x^2 + 2\Delta y v_0^2)}}{g x} \quad (7)$$

where

θ = launch angle (deg)
v_0 = initial velocity / muzzle velocity (m/s)
x = horizontal distance to the target (m)
Δy = vertical distance (m)
g = gravitational acceleration (9.81 m/s²)

With an initial velocity of 6.445 m/s, the trajectory equation yields two possible solutions for the launch angle: 31.37° or 78.77°. The lower angle was selected to minimize the time of flight. Additionally, we used MATLAB to simulate various trajectories to analyze target height and trajectory deviations.

The results show that angles slightly below the computed solution (e.g., 25°–30°) produce a trajectory that remains below the target height at x = 1.5 m, resulting in an undershoot. For instance, at $\theta = 25°$ the predicted height is $y(1.5) \approx 0.375$ m, and at $\theta = 27°$, it is $y(1.5) \approx 0.430$ m; both are significantly lower than the required 0.55 m. Therefore, even angles close to 31° remain insufficient to hit the target unless they are within a narrow range around the calculated optimum.

To enhance mechanical reliability and power efficiency, the active servo-driven reload system has been replaced with a passive gravity-assisted mechanism. By reconfiguring the ball stock to a 90-degree orientation relative to the deck surface and contouring it to the ball's geometry, the system ensures consistent feeding without the need for electronic actuation.

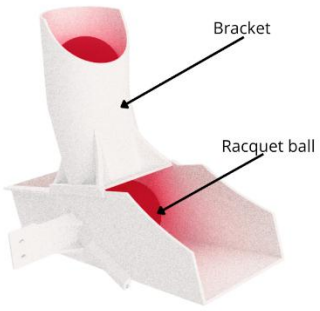

Fig. 1. Ball launcher design.

III. Water Shooter

To generate greater pressure and velocity than the previous design (pressure of 4.97 kPa and velocity of 3.16 m/s), we reduced the diameter of the water inlet to 0.86 cm, resulting in a pressure of 151 kPa and a velocity of 17 m/s. These

pressure and velocity values were obtained using the formula below:

$$P = P_{wf} + P_{hf} + P_{y\text{-connector}}$$

$$P_{wf} = P_{\text{without friction}}$$

$$P_{hf} = P_{\text{hose friction}}$$

The pressure Pwf of 140 kPa was obtained from the following calculation:

$$P_{wf} = \frac{1}{2}\rho(v_{out}^2 - v_{in}^2)$$

$$v_{out}^2 = 16.98\ \text{m/s}$$

$$v_{in}^2 = 2.87\ \text{m/s}$$

Then the pressure from the hose friction is 11.97 kPa from the calculation below:

$$P_{hf} = f\left(\frac{L}{d}\right)\left(\frac{1}{2}\rho v_{in}^2\right)$$

$$f = friction\ factor = 0.025$$

$$L = 1\ \text{m}$$

$$d = 0.086\ \text{cm}$$

Then, the pressure from the Y-connector resistance is 3.088 kPa from the calculation below

$$P_{y\text{-connector}} = K\left(\frac{1}{2}\rho v_{in}^2\right)$$

$$K = resistance\ coefficient = 0.75$$

We also analyzed the design with the new inlet diameter configuration using ANSYS Fluent software. The results of this analysis showed slightly different results from the manual calculations as shown in Table I. below:

TABLE I. WATER SHOOTER CALCULATION ANALYSIS

Parameter	**Analysis Type**	
	Manual	***CFD (Fluent)***
Pressure (kPa)	150.101	151
Velocity (m/s)	17	17

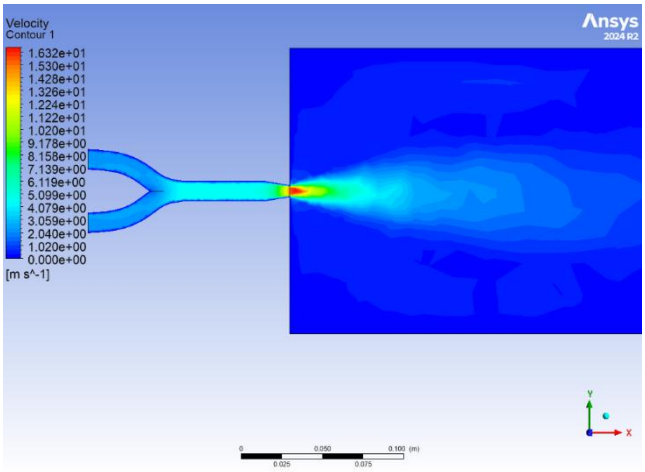

Fig. 2. Water shooter analysis.

In these results, there is a difference where the pressure in CFD analysis results is greater than the manual calculations, but the velocities are the same.

IV. MICROPHONE

The objective of this test is to validate the acoustic system's capability to detect and classify 'Harbor Alert' sound signals in real-time. The system must accurately distinguish between three fundamental frequencies (600 Hz, 800 Hz, and 1000 Hz) and two distinct blast patterns (Pattern A and Pattern B) under various environmental noise conditions. The set up and environmental conditions for the test are:

1) *Hardware:* Logitech Brio 500 (Integrated Microphone) interfaced with an Intel NUC for onboard processing.

2) *Audio Source:* HK ONYX 4 Speaker (100% volume).

3) *Distance:* Variable range between 1 to 20 meters.

4) *Software:* Preliminary analysis conducted via MATLAB; real-time processing implemented using a Neural Network on ROS 2.

The testing procedures can be explained in these points:

1) Spectral analysis: Conducting spectral characterization using spectrograms to verify active blast durations and inter-blast gaps.

2) Dataset preparation: Utilizing 180 sound samples with amplitude variations (10% - 100%) and synthetic noise augmentation to enhance model adaptivity.

3) Comparative testing: Benchmarking the performance of conventional Spectrogram-based features against Mel-Frequency Energy (MFE) features.

4) Operational validation (on-water trial): Field testing the system during autonomous mission cycles to evaluate the impact of motor noise and aquatic environmental interference.

The following tables compare the performance results between the initial spectrogram method and the optimized MFE method:

TABLE II. PERFORMANCE RESULTS USING SPECTROGRAM FEATURES

Test Data	Sample	True	False	Acc (%)	Note
Sample Sound	180	180	0	100	-
Sample Sound with Noise	180	176	4	97,7	3 600Hz_B, 1 800Hz_B
Real Time MIC	30	27	3	90	3 600Hz_B
On Trial	24	19	6	79,16	4 600Hz_B, 2 800Hz_B

TABLE III. PERFORMANCE RESULTS USING MFE

Test Data	Sample	True	False	Acc (%)	Note
Sample Sound	180	180	0	100	-
Sample Sound with Noise	180	177	3	98,3	3 600Hz_B,
Real Time MIC	30	28	2	93,3	2 600Hz_B
On Trial	24	23	1	95,8	3 600Hz_B,

Initial testing indicated that conventional spectrogram features suffered from a time-frequency resolution trade-off, leading to ‘blurring’ of the short inter-blast gaps (0.5 seconds) in Pattern B, particularly at lower frequencies (600 Hz). The transition to MFE features improved temporal resolution and classification accuracy under low Signal-to-Noise Ratio (SNR) conditions, increasing operational accuracy from 79.16% to 95.8%. While minor misclassifications still persist for the 600Hz_B pattern, current efforts are focused on iterative model refinement and alternative deep learning architectures to ensure peak reliability during competition day.

Appendix E: Object Detection Performance Analysis

I. Introduction

To ensure the highest reliability in mission performance, the team conducted extensive testing to compare several object detection architectures. This analysis evaluates both Convolutional Neural Network (CNN) based models, represented by the YOLO family, and Transformer-based architectures, represented by DETR variants. The primary objective was to identify the most balanced model that satisfies the best accuracy and real-time inference requirements (FPS) of the competition.

II. Technical Analysis And Model Selection

A. Testing Methodology

All models were trained and tested using the same competition-specific dataset to maintain evaluation consistency. To accommodate our demanding development timeline, training parameters were standardized across models with the exception of epoch count. It was observed that training the DETR architecture for 70 epochs required the same temporal overhead as training YOLO for 200 epochs (approximately 1.5 hours). Consequently, this trade-off was used to ensure all models were compared within a feasible training window.

B. Performance Metrics and Results

Performance was measured across four primary metrics: F1-Score, FPS (tested on CPU), mAP50, and mAP50-95. The raw data from these tests are summarized in Table I.

Table I. Object Detection Model Evaluation Results

Model	F1-Score	FPS	mAP50	mAP50-95
YOLOv8n	0.9209	58.87	0.9592	0.7836
YOLOv9t	0.9213	54.33	0.9595	0.7839
YOLOv11n	0.9133	60.44	0.9570	0.7726
YOLOv10n	0.9174	55.91	0.9593	0.7819
YOLOv12n	0.9184	33.31	0.9504	0.7815
RT-DETRr18vd	0.7549	8.15	0.8775	0.6032
LW-DETRt	0.8666	6.16	0.9135	0.7041

C. Weighted Normalization and Selection

A data normalization method was implemented to find the most balanced operational score, using an equal weighting of 25:25:25:25 across the primary metrics. This prevented any single metric from disproportionately influencing the final decision.

Table II. Normalized Object Detection Performance

Model	Norm F1-Score	Norm FPS	Norm mAP50	Norm mAP50-95	Total Score
YOLOv8n	0.997	0.971	0.996	0.998	0.991
YOLOv9t	1.000	0.887	1.000	1.000	0.972
YOLOv11n	0.976	0.917	0.997	0.988	0.970
YOLOv10n	0.951	1.000	0.969	0.937	0.965
YOLOv12n	0.982	0.500	0.889	0.986	0.840
RT-DETRr18vd	0.671	0.000	0.439	0.558	0.417
LW-DETRt	0.000	0.037	0.000	0.000	0.009

III. Conclusion

YOLOv8n was selected as the optimal architecture due to its greater speed and accuracy. While DETR models demonstrated high precision. they suffered from poor recall and a higher rate of false negatives caused by the dataset's null filter. Although DETR remains a candidate for future development with refined dataset filtering. YOLOv8n remains to be our selected model for our vessels.